Journal of Theoretical Biology 406 (2016) 124–128

Contents lists available at ScienceDirect

Journal of Theoretical Biology

journal homepage: www.elsevier.com/locate/yjtbi

Gray level co-occurrence matrix algorithm as pattern recognition biosensor for oxidopamine-induced changes in lymphocyte chromatin architecture

Igor Pantic [a,*], Draga Dimitrijevic [b], Dejan Nesic [a], Danica Petrovic [c]

[a] Laboratory for cellular physiology, Institute of medical physiology, School of medicine, University of Belgrade, Visegradska 26/II, RS-11129 Belgrade, Serbia
[b] Hospital Laza Lazarevic, Visegradska 26, RS-11129 Belgrade, Serbia
[c] Health Center Studenica, Kraljevo, Jug Bogdanova 112, RS-36000 Kraljevo, Serbia

HIGHLIGHTS

- Peripheral blood was treated with 6-hydroxydopamine.
- The smears were stained using a modification of Feulgen method for DNA visualization.
- 120 chromatin structures were analyzed GLCM mathematical algorithm.
- 6-hydroxydopamine induced the rise of the values of chromatin GLCM entropy and variance.

ARTICLE INFO

Article history:
Received 8 April 2016
Received in revised form
10 June 2016
Accepted 13 July 2016
Available online 16 July 2016

Keywords:
Dopamine
Blood
Homogeneity
Image analysis
Pattern

ABSTRACT

We demonstrate that a proapoptotic chemical agent, oxidopamine, induces dose dependent changes in chromatin textural patterns which can be quantified using the Gray level co-occurrence matrix (GLCM) method. Peripheral blood (heparin-pretreated) samples were treated with oxidopamine (6-OHDA, 6-hydroxydopamine) to achieve effective concentrations of 100, 200 and 300 μM. The samples were smeared on microscope slides and fixated in methanol. The smears were stained using a modification of Feulgen method for DNA visualization. For each stained smear, a sample of 30 lymphocyte chromatin structures were visualized and analyzed. This way, textural parameters for a total of 120 nuclei micrographs were calculated. For each chromatin structure, five different GLCM features were calculated: angular second moment, GLCM entropy, inverse difference moment, GLCM correlation, and GLCM variance. Oxidopamine induced the rise of the values of GLCM entropy and variance, and the reduction of angular second moment, correlation, and inverse difference moment. The trends for GLCM parameter changes were found to be highly significant ($p < 0.001$). These results indicate that GLCM mathematical algorithm might be successfully used in detection and evaluation of discrete early apoptotic structural changes in Feulgen-stained chromatin of peripheral blood lymphocytes that are not detectable using conventional microscopy/cell biology techniques.

1. Introduction

In recent years, there have been many attempts to design and implement a mathematical image analysis method capable of quantifying changes in cell and tissue structure during various physiological and pathological processes. Some of these algorithms, such as texture analysis methods, were in some cases able to successfully evaluate properties of chromatin distribution during programmed cell death and aging (Losa and Castelli, 2005; Pantic et al., 2012a; 2012b).

Of all texture analysis techniques, today probably the most widely used is the one based on gray level co-occurrence matrix (GLCM) algorithm. GLCM method was first proposed by Haralick et al. (1973) as a way to classify images using second order statistical measurements. Recently, many laboratories have applied GLCM in biological systems, for assessment of some important structural features, such as homogeneity, uniformity and level of disorder (Pantic et al., 2013; Shamir et al., 2009).

Today, for GLCM analysis in histology and pathology, the tissue micrographs are usually converted to gray scale (i.e. 8 bit) format,

* Corresponding author.
E-mail address: igor.pantic@mfub.bg.ac.rs (I. Pantic).

http://dx.doi.org/10.1016/j.jtbi.2016.07.018
0022-5193/

after which individual resolution units are assigned a numerical value that quantifies their gray intensity. Second order statistics is applied in order to analyze resolution unit pairs, which are formed according to the predetermined distance and angle in the micrograph. This way, many textural features can be calculated, among which most important may be: angular second moment (ASM), GLCM correlation, entropy, inverse difference moment and GLCM variance (Pantic et al., 2014). For example, inverse difference moment may be an indirect parameter of textural homogeneity, whereas the angular second moment may be an indicator of gray level uniformity. Entropy is a measure of textural disorder within the analyzed structure.

Some GLCM features were suggested to be important quantifiers of chromatin structure. Our recent research has demonstrated that chromatin GLCM entropy of some spleen progenitor (stem) cells increases as the result of physiological aging (Pantic et al., 2012a). In another study, we demonstrated that lymphocytes in thymus cortex and medulla exhibit different values of nuclear entropy, angular second moment, variance and texture correlation (Pantic et al., 2013). These findings represent indirect proof that GLCM method is sensitive in spotting discrete structural changes of lymphocyte chromatin that are otherwise undetectable using conventional morphometric techniques in microscopy.

Particularly important area with potentially high applicability of GLCM method is apoptosis research (Losa and Castelli, 2005). In our previous study we concluded that entropy and inverse difference moment could in the future become important determinants of chromatin condensation and marginalization during early stages of lymphocyte apoptosis (Pantic et al., 2012b). Losa and Castelli also indicated that certain GLCM features could be sensitive parameters of chromatin ultrastructural changes during programmed cell death. It seems that in apoptosis detection, some of these features could even be more sensitive than gold standard conventional methods, such as fluorescence-activated cell sorting.

In this study we tested the ability of GLCM method to detect structural alterations in lymphocyte chromatin after treatment with oxidopamine as a toxin. We show that this toxin in a dose-dependent manner, changes some GLCM parameters, such as angular second moment, entropy, variance, and correlation. We also show that certain GLCM parameters have excellent discriminatory ability in distinguishing oxidopamine-treated from untreated cells.

2. Material and methods

2.1. Experimental protocol and Feulgen staining

Peripheral blood (heparin-pretreated) obtained from a healthy donor (IP) was treated with Oxidopamine (6-OHDA, 6-hydroxydopamine) to achieve effective concentration of 100, 200 and 300 μM. 120 min after the treatment the samples were smeared on microscope slides and fixated in methanol. The smears were stained using a modification of Feulgen method for DNA visualization (Hardie et al., 2002). Briefly, after the methanol fixation, and washing with deionized water, the smears were treated with 5N hydrochloric acid for 120 min, and subsequently with 0.1N hydrochloric acid. The staining of cells was then done using Schiff's reagent (prepared using basic fuchsin and sodium metabisulfite). The staining was done in the dark, and its duration was 120 min. The smears were then rinsed 3×5 min with bisulfite (10% aqueous sodium metabisulphite 6 ml, 1N hydrochloric acid 5 ml, distilled water to 100 ml), and 3×2 min with distilled water. For details on Feulgen method, the reader is referred to the previously published work (Hardie et al., 2002).

For each stained smear, a sample of 30 lymphocyte chromatin structures were visualized and analyzed. This way, textural parameters for a total of 120 nuclei (for 3 OHDA treated samples + control sample) were calculated. Digital micrographs of the cells (Fig. 1) were created using DEM 200 High-Speed Color CMOS Chip DC 5 V/250 mA (Oplenic Optronics, Hangzhou, CN) mounted on Olympus CX21FS1 microscope (1000 × magnification). The Regions of Interest (ROIs) of the lymphocyte nuclei were marked using ImageJ software (National Institutes of Health, Bethesda, Maryland). The ROIs were analyzed directly from the micrographs without the cropping or any additional modifications.

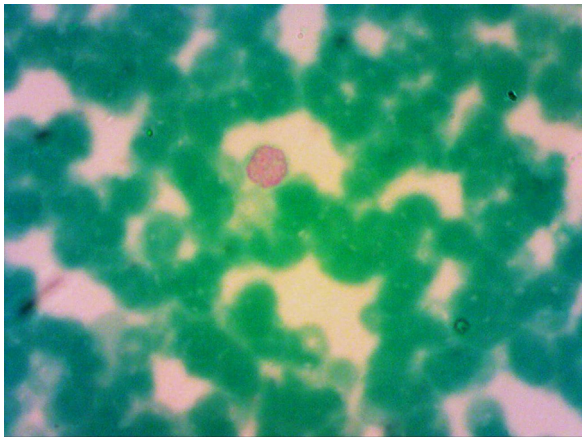

Fig. 1. An example of micrograph depicting Feulgen-stained cells with a lymphocyte at the center. The technique is based on hydrolysis of DNA molecule which is stained red. In standard blood smears, leukocyte nuclei are stained red while other elements, such as leukocyte cytoplasm and erythrocytes are stained green. (For interpretation of the references to color in this figure legend, the reader is referred to the web version of this article.)

2.2. Gray level co-occurrence matrix (GLCM) analysis

GLCM analysis of nuclear chromatin ROIs was done with ImageJ plugins Texture Analyzer (Cabrera, 2005), GLCM_TextureToo (Cornish, 2007) and MATLAB software code (MathWorks, Natick, Massachusetts, USA) for. Prior to analysis, the micrographs were converted to 8-bit format in ImageJ. For each chromatin structure, five different GLCM features were quantified: angular second moment (ASM), GLCM entropy (ENT), inverse difference moment (IDM), GLCM correlation (COR), and GLCM variance (VAR).

Angular second moment (indicator of texture uniformity), was calculated as:

$$\mathrm{ASM}=\sum_{\mathrm{i}}\sum_{\mathrm{j}}\left\{\mathrm{p}(\mathrm{i},\mathrm{j})\right\}^2$$

where i and j are the gray values/coordinates in co-occurrence matrix, μ is mean and σ standard deviation determined from pixel pair values ($p(i,j)$). For the details regarding GLCM protocol, the reader is referred to the original paper where the method is explained (Haralick R, 1973) as well as other publications about GLCM method (Loizou et al., 2014; Maani et al., 2014; Pantic et al., 2012b; Song et al., 2013).

GLCM Inverse difference moment (indirect indicator of homogeneity), was calculated based on the formula:

$$\mathrm{IDM}=\sum_{\mathrm{i}}\sum_{\mathrm{j}}\frac{1}{1+(\mathrm{i}-\mathrm{j})^2}\mathrm{p}(\mathrm{i},\mathrm{j})$$

GLCM variance (indirect measure of heterogeneity) was determined as:

$$\mathrm{VAR}=\sum_{i}\sum_{j}(i-\mu)^2 p(i,j)$$

GLCM correlation was quantified as:

$$\mathrm{COR} = \frac{\sum_i \sum_j (ij)p(i,j) - \mu_x \mu_y}{\sigma_x \sigma_y}$$

Finally, GLCM entropy (indicator of textural disorder) was determined as:

$$\mathrm{ENT} = -\sum_i \sum_j p(i,j) \log\,(p(i,j))$$

3. Results

Average chromatin entropy was 5.47 ± 0.27 in control cells, and after OHDA treatment it increased to 5.57 ± 0.27 (100 μM), 5.66 ± 0.30 (200 μM) and 6.15 ± 0.38 (300 μM). The increase was dose-dependent, and statistically significant positive trend was observed ($p < 0.01$, Fig. 2). When post-hoc statistical analysis was performed, it was determined that the first significant increase occurred in 300 μM sample.

Average chromatin GLCM variance in the control sample was 51.75 ± 36.22 (Fig. 2). Oxidopamine-treated samples had average variance values of 67.62 ± 66.81, 81.53 ± 63.80 and 178.23 ± 106.17, respectively. The increase in the 300 μM sample compared to control was so significant ($p < 0.001$), that when

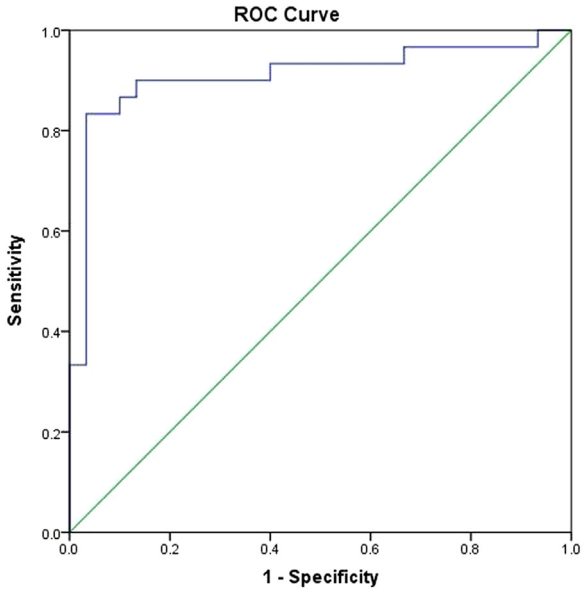

Fig. 3. Receiver operating characteristic (ROC) curve for GLCM variance. This parameter had an outstanding discriminatory power for OHDA-treated (300 μM) and untreated cells. The area under the ROC curve was 0.91.

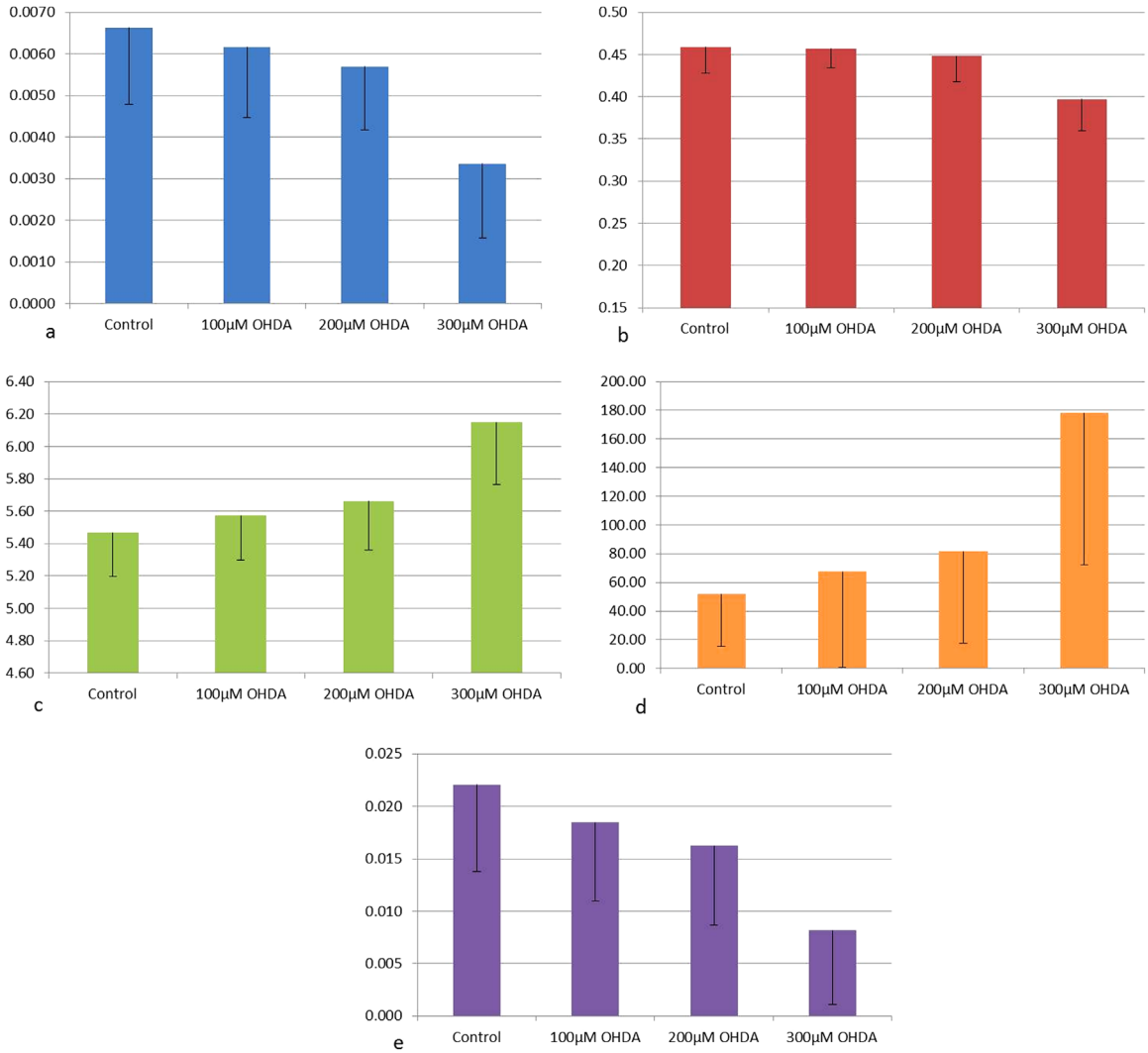

Fig. 2. Mean values of angular second moment (a), inverse difference moment (b), GLCM entropy (c), GLCM variance (d), and GLCM correlation (e).

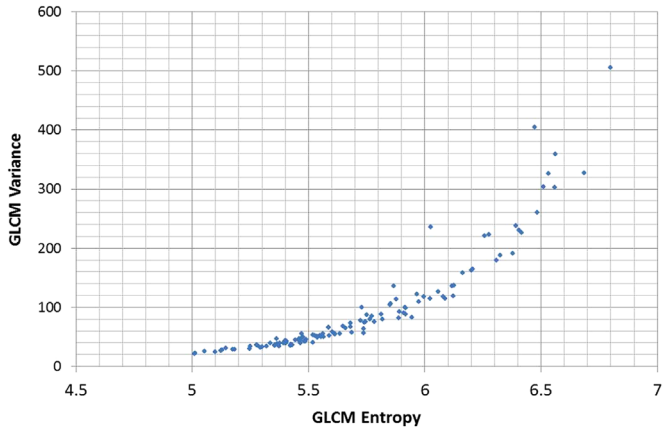

Fig. 4. Plotted values of GLCM variance and entropy. Statistically highly significant correlation between the two parameters was observed ($p < 0.001$).

Receiver operating characteristic (ROC) analysis was performed, GLCM variance had an outstanding discriminatory power between the two samples. The area under the ROC curve was 0.91, with sensitivity of 96.7% for the VAR values equal or higher than 21.66 (Fig. 3). There was a statistically highly significant positive correlation between entropy and variance values both in experimental and control groups of cells. The diagram showing the plotted values of both parameters is presented in Fig. 4.

Mean values of chromatin inverse difference moment did not significantly change until the samples were treated with 300 μM OHDA. In the control sample, mean IDM equaled 0.46 ± 0.03, whereas in the first two experimental samples its values were 0.46 ± 0.02 and 0.45 ± 0.0, respectively. In the 300 μM sample, IDM significantly decreased to 0.40 ± 0.04.

GLCM correlation significantly decreased after treatment with OHDA in a dose-dependent manner. In the control sample, the average value of chromatin GLCM correlation was 0.022 ± 0.008. In experimental groups, the values of GLCM correlation were 0.018 ± 0.007, 0.016 ± 0.008, and 0.008 ± 0.007, respectively, which was a statistically significant dose-dependent reduction. Statistically significant ($p < 0.01$) negative trend was observed.

Finally, angular second moment of the co-occurrence matrix also exhibited substantial reduction after OHDA treatment. In the control group of chromatin structures, its mean value was 0.0066 ± 0.0018, while in experimental groups, it was 0.0062 ± 0.0017, 0.0057 ± 0.0015, and 0.0034 ± 0.0018, respectively. Similarly as with GLCM correlation, statistically significant ($p < 0.01$) negative trend was observed.

4. Discussion

In this article we present results that a proapoptotic chemical agent, oxidopamine, changes the parameters of lymphocyte chromatin texture in a dose dependent manner. The texture was quantified using the features of Gray level co-occurrence matrix, and oxidopamine induced the increase of the values of GLCM entropy and variance, and the reduction of angular second moment, correlation, and inverse difference moment. Using the conventional statistical analytical tests, the trends of GLCM parameter changes were found to be highly significant. These findings indicate that GLCM as a method, is capable of detecting discrete structural changes in lymphocyte chromatin associated with early stages of apoptosis, that are otherwise undetectable during standard light microscopy evaluation.

Oxidopamine is a known neurotoxin, and it is often used in neuroscience research for the design of animal experimental models resembling Parkinson's and other neurological diseases (Aguiar et al., 2013; Chong et al., 2013; Gu et al., 2013; Ham et al., 2013; Koizumi et al., 2013; Kuruvilla et al., 2013; Tovilovic et al., 2013). In lymphocytes, oxidopamine in concentrations similar to the ones used in our research may induce apoptosis within 24 hours (Del Rio and Velez-Pardo, 2002). During the process of programmed cell death many morphological changes occur in the cell nucleus. Chromatin becomes more condense, and sometimes is marginalized near the nuclear envelope. DNA fragmentation also takes place and it can be measured using the conventional cytofluorometric methods, such as Fluorescence-activated cell sorting (FACS) after proper labeling.

Probably the most important finding of our study was the outstanding discriminatory ability of GLCM variance in distinguishing oxidopamine-treated cells from normal cells. This parameter had an unusually high sensitivity of more than 95%, and a large area under the receiver operating characteristic curve of 0.91. In other words, GLCM variance alone, independently from other textural features, was highly accurate in identifying the altered chromatin structure.

Losa and Castelli (2005) conducted a study on apoptosis in which they demonstrated that GLCM method is particularly useful in chromatin analysis. The study was done on breast cancer cell line, using transmission electron microscopy. Apoptosis was induced with a toxic compound calcimycin, and during the early stages of the process, fractal, GLCM and cytofluorometric analyses were performed. The authors concluded that certain GLCM features may be more sensitive in apoptosis detection when compared to conventional methods. GLCM variance, similarly as in our study, was shown to be a particularly valuable parameter (Losa and Castelli, 2005).

Another potentially important result of our research is the statistically highly significant rise of chromatin GLCM entropy in damaged chromatin structure. Entropy as a measure of chaos and disorder was often implicated to be an important parameter of structural degradation and deterioration. For example, Shamir et al. (2009) described GLCM entropy in muscle tissue as an important parameter of age-related degenerative changes (Shamir et al., 2009). Our previous study in hematopoietic tissue also showed an age-related increase of chromatin entropy (Pantic et al., 2012a). Our work provides a modest contribution to the present knowledge on this textural feature and its applicability in cell biology.Our study has several potential implications. First, if these results are confirmed in the future, certain GLCM parameters could become an important addition to the current gold standard methods for early apoptosis detection. Second, these results confirm past observations that GLCM as a method is capable of quantifying even minor structural changes in chromatin architecture in Feulgen stained cells. Using the contemporary mathematical and information technology techniques, perhaps it would be possible to design a novel image analysis method combining GLCM features to achieve even greater sensitivity and accuracy. It should also be noted that the methodology used in this research is relatively exact, and is not subject to inter or intra observer variability. In fact, our previous studies tested inter-observer reliability of the method and determined it to be very high. Another important advantage of the method is that it can be performed using freely-available (public domain) software, such as the ImageJ and its plugins designed by NIH. The method also does not require significant material resources such as FACS equipment nor substantial molecular biology expertize.

5. Conclusion

In conclusion, our study demonstrates that a proapoptotic chemical agent, oxidopamine, induces dose dependent changes in

chromatin textural patterns which can be quantified using the Gray level co-occurrence matrix method. This mathematical algorithm can be successfully used in detection and evaluation of discrete early apoptotic structural changes in Feulgen-stained chromatin of peripheral blood lymphocytes that are not detectable using conventional microscopy/cell biology techniques.

Acknowledgments

The authors are grateful to the project 62013 of the Mediterranean Society for Metabolic Syndrome, Diabetes and Hypertension in Pregnancy DEGU, as well as to the projects of The Ministry of Education and Science, Republic of Serbia (175059 and 41027). The author also acknowledges technical help from National Institutes of Health (Bethesda, MD) regarding the function of the image analysis software, as well the technical help received by Prof. Dr. Senka Pantic from the Department of Histology during the experiments.

References

Aguiar Jr., A.S., Moreira, E.L., Hoeller, A.A., Oliveira, P.A., Cordova, F.M., Glaser, V., Walz, R., Cunha, R.A., Leal, R.B., Latini, A., Prediger, R.D., 2013. Exercise attenuates levodopa-induced dyskinesia in 6-hydroxydopamine-lesioned mice. Neuroscience 243, 46–53. http://dx.doi.org/10.1016/j.neuroscience.2013.03.039.

Cabrera, J., 2005. Texture Analyzer. http//rbs.Info.nih.gov/ij/plugins/texture.html.

Chong, C.M., Zhou, Z.Y., Razmovski-Naumovski, V., Cui, G.Z., Zhang, L.Q., Sa, F., Hoi, P. M., Chan, K., Lee, S.M., 2013. Danshensu protects against 6-hydroxydopamine-induced damage of PC12 cells in vitro and dopaminergic neurons in zebrafish. Neurosci. Lett. 543, 121–125. http://dx.doi.org/10.1016/j.neulet.2013.02.069.

Cornish, T.B., 2007. GLCM_TextureToo. http://tobycornish.com/downloads/imagej/.

Del Rio, M.J., Velez-Pardo, C., 2002. Monoamine neurotoxins-induced apoptosis in lymphocytes by a common oxidative stress mechanism: involvement of hydrogen peroxide (H(2)O(2)), caspase-3, and nuclear factor kappa-B (NF-kappaB), p53, c-Jun transcription factors. Biochem. Pharmacol. 63, 677–688.

Gu, H., Wang, J., Du, N., Tan, J., Johnstone, B., Du, Y., 2013. Adipose stromal cells-conditioned medium blocks 6-hydroxydopamine-induced neurotoxicity and reactive oxygen species. Neurosci. Lett. 544, 15–19. http://dx.doi.org/10.1016/j.neulet.2013.02.057.

Ham, A., Kim, D.W., Kim, K.H., Lee, S.J., Oh, K.B., Shin, J., Mar, W., 2013. Reynosin protects against neuronal toxicity in dopamine-induced SH-SY5Y cells and 6-hydroxydopamine-lesioned rats as models of Parkinson's disease: reciprocal up-regulation of E6-AP and down-regulation of alpha-synuclein. Brain Res. 1524, 54–61. http://dx.doi.org/10.1016/j.brainres.2013.05.036.

Haralick, R., S. K, Dinstein, I., 1973. Textural features for image classification. IEEE Trans. Syst. Man Cybern. SMC-3, 610–621.

Hardie, D.C., Gregory, T.R., Hebert, P.D., 2002. From pixels to picograms: a beginners' guide to genome quantification by feulgen image analysis densitometry. J. Histochem. Cytochem. 50, 735–749.

Koizumi, H., Morigaki, R., Okita, S., Nagahiro, S., Kaji, R., Nakagawa, M., Goto, S., 2013. Response of striosomal opioid signaling to dopamine depletion in 6-hydroxydopamine-lesioned rat model of Parkinson's disease: a potential compensatory role. Front. Cell. Neurosci. 7, 74. http://dx.doi.org/10.3389/fncel.2013.00074.

Kuruvilla, K.P., Nandhu, M.S., Paul, J., Paulose, C.S., 2013. Oxidative stress mediated neuronal damage in the corpus striatum of 6-hydroxydopamine lesioned Parkinson's rats: neuroprotection by serotonin, GABA and bone marrow cells supplementation. J. Neurol. Sci. 331, 31–37. http://dx.doi.org/10.1016/j.jns.2013.04.020.

Loizou, C.P., Petroudi, S., Seimenis, I., Pantziaris, M., Pattichis, C.S., 2014. Quantitative texture analysis of brain white matter lesions derived from T2-weighted MR images in MS patients with clinically isolated syndrome. J. Neuroradiol. . http://dx.doi.org/10.1016/j.neurad.2014.05.006

Losa, G.A., Castelli, C., 2005. Nuclear patterns of human breast cancer cells during apoptosis: characterisation by fractal dimension and co-occurrence matrix statistics. Cell Tissue Res. 322, 257–267. http://dx.doi.org/10.1007/s00441-005-0030-2.

Maani, R., Kalra, S., Yang, Y.H., 2014. Robust volumetric texture classification of magnetic resonance images of the brain using local frequency descriptor. IEEE Trans. Image Process. . http://dx.doi.org/10.1109/TIP.2014.2351620

Pantic, I., Pantic, S., Paunovic, J., 2012a. Aging increases nuclear chromatin entropy of erythroid precursor cells in mice spleen hematopoietic tissue. Microsc. Microanal. 18, 1054–1059. http://dx.doi.org/10.1017/S1431927612001377.

Pantic, I., Pantic, S., Basta-Jovanovic, G., 2012b. Gray level co-occurrence matrix texture analysis of germinal center light zone lymphocyte nuclei: physiology viewpoint with focus on apoptosis. Microsc. Microanal. 18, 470–475. http://dx.doi.org/10.1017/S1431927612000098.

Pantic, I., Pantic, S., Paunovic, J., Perovic, M., 2013. Nuclear entropy, angular second moment, variance and texture correlation of thymus cortical and medullar lymphocytes: grey level co-occurrence matrix analysis. An. Acad. Bras. Cienc. 85, 1063–1072. http://dx.doi.org/10.1590/S0001-37652013005000045.

Pantic, I., Dacic, S., Brkic, P., Lavrnja, I., Pantic, S., Jovanovic, T., Pekovic, S., 2014. Application of fractal and grey level co-occurrence matrix analysis in evaluation of brain corpus callosum and cingulum architecture. Microsc. Microanal. 20, 1373–1381. http://dx.doi.org/10.1017/S1431927614012811.

Shamir, L., Wolkow, C.A., Goldberg, I.G., 2009. Quantitative measurement of aging using image texture entropy. Bioinformatics 25, 3060–3063. http://dx.doi.org/10.1093/bioinformatics/btp571.

Song, C.I., Ryu, C.H., Choi, S.H., Roh, J.L., Nam, S.Y., Kim, S.Y., 2013. Quantitative evaluation of vocal-fold mucosal irregularities using GLCM-based texture analysis. Laryngoscope. http://dx.doi.org/10.1002/lary.24151.

Tovilovic, G., Zogovic, N., Soskic, V., Schrattenholz, A., Kostic-Rajacic, S., Misirkic-Marjanovic, M., Janjetovic, K., Vucicevic, L., Arsikin, K., Harhaji-Trajkovic, L., Trajkovic, V., 2013. Arylpiperazine-mediated activation of Akt protects SH-SY5Y neuroblastoma cells from 6-hydroxydopamine-induced apoptotic and autophagic death. Neuropharmacology 72, 224–235. http://dx.doi.org/10.1016/j.neuropharm.2013.04.037.